Supplementary Material to the article
"Infrared transmission spectra of TiS_3:
fundamental absorption edge, phonons and excitons"

Far-IR transmittance of TiS_3.

Fig. S1a shows the transmission spectra of a TiS_3 single crystal of unpolarized radiation, as well as radiation with polarization of the electric field **E** along the **a** and **b** axes. The wavelengths are in the far infrared range and match the energy region of excitation of optically active phonons. The crystal structure of titanium trisulfide is P21/m (#11), 2 formula units per unit cell. In this case, 24 phonon modes are possible, 3 of them are acoustic. Possible representations: Ag, Au, Bg and Bu, of which the optically active ones are 3Au and 6Bu. Table S1 shows the values of the absorption band maxima. Some of the bands have previously been observed in reflectance or transmission spectra and have been identified in the literature [1,2]. Note that in the transmission spectrum measured at room temperature (Fig. 1b), not all bands observed in [1,2] are visible, which is associated with strong absorption on free carriers. As the temperature decreases, a number of additional weak absorption lines appear. In addition, narrowing of the phonon bands can be seen (Fig. S1b), but no significant changes in the spectrum that could indicate a structural phase transition are observed.

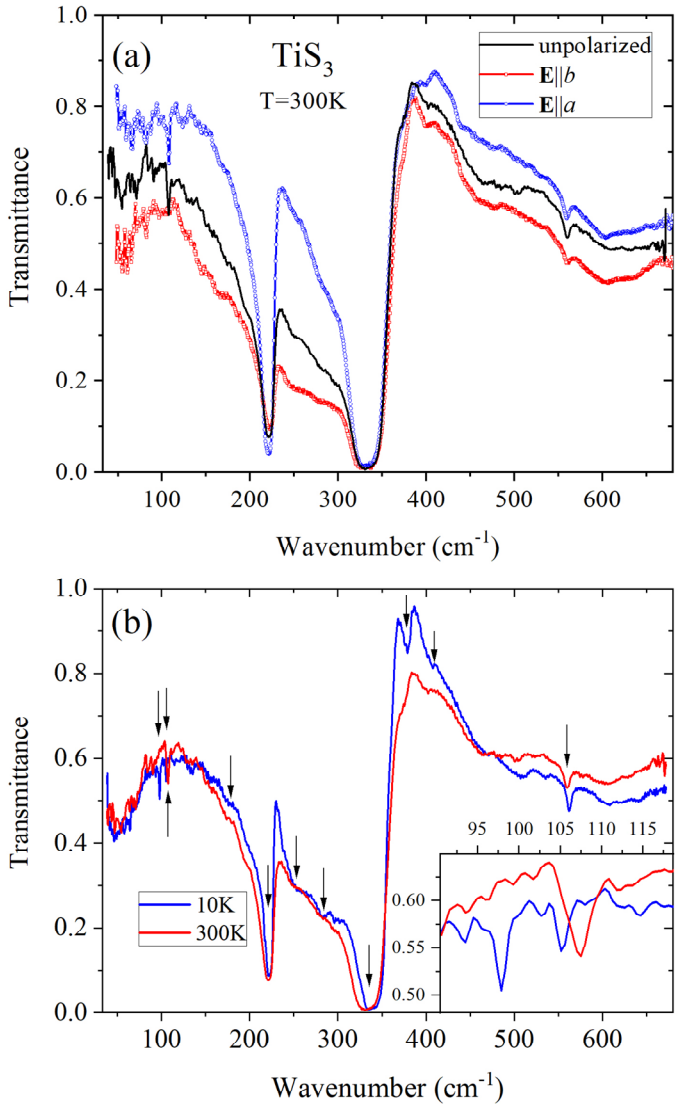

Fig. S1. Transmission spectra of TiS_3 single crystal # 1: (a) at T=300 K in unpolarized and linearly polarized light; (b) at T=300 K and 10 K in unpolarized light. **Inset**: fragments of the same spectra in the region of 70-150 cm^{-1}. The arrows indicate absorption lines.

Table S1. Absorption bands observed in the spectra.

	Optical phonon frequencies (cm^{-1})					
	Results of the present work				[1]	[2]
	Unpolarized light		**E ∥ a**	**E ∥ b**		
	300 K	10 K	300 K	300 K		
	107	105 97	107	107 96		104 (A_g) (Raman phonon) (in ZnS_3 and HfS_3 –B_u symmetry)
	176	178		169	177 (A_u)	
	221	222	221	222	217 (B_u)	217 (A_u)
	250	252	253	246		
	278	282	280	278	276 (B_u)	276 (B_u)
					295 (A_u)	295 (A_u)
					309 (B_u)	309 (B_u)
	322-344	331-348	322-342	320-344	333 (B_u)	333 (B_u)
	375	377	375	375		
	402	407	400	400		400 (B_u)
	560	562	560	560		560 (B_u)

Tauc plots and the nature of the interband transitions.

To determine the type of interband transitions that form the absorption edge, we replotted the experimental points in coordinates $(D\mathscr{E})^n$ vs. $\mathscr{E}$ for n=2 or 1/2, that is, we constructed Tauc plots [3]. If the dependence near the edge is straightened at n=2, the transitions are direct and allowed; if at n=1/2, the transitions are indirect and allowed [3]. Fig. S2 presents experimental data for both values of n. Fig. S2b shows regions that are linear over a wider energy range than in Fig. S2a, which indicates the indirect nature of the transitions.

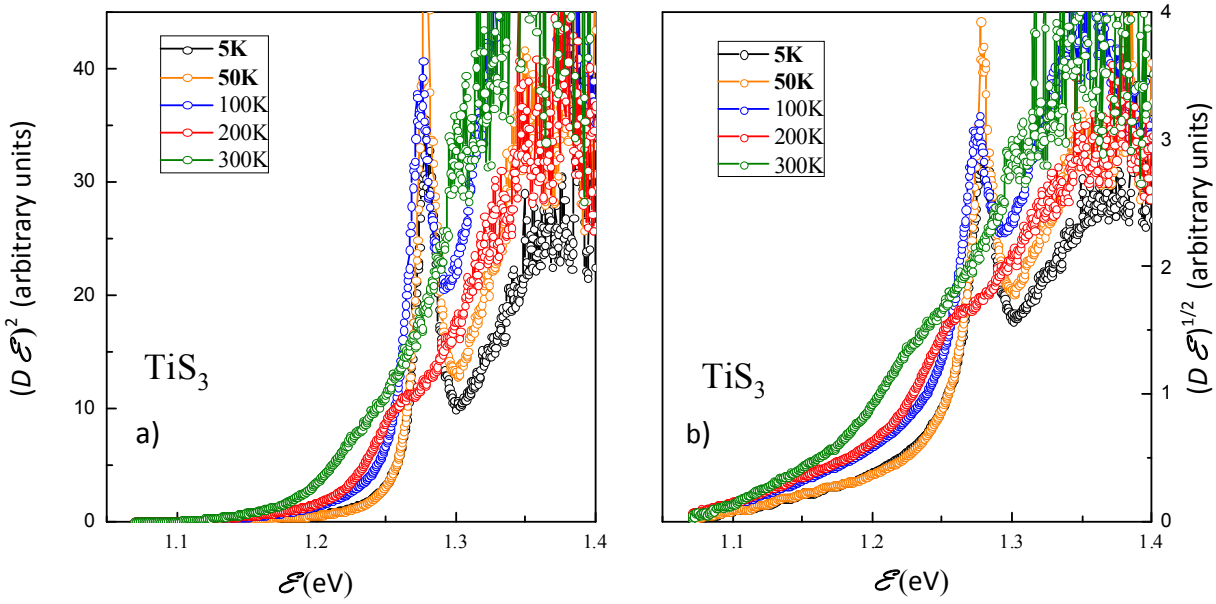

Fig. S2. Optical density spectra of single crystal # 1 (see Fig. 2b) in the coordinates $(D\mathscr{E})^2$ vs $\mathscr{E}$ (a) and $(D\mathscr{E})^{1/2}$ vs $\mathscr{E}$ (b).

However, the analysis of transmission spectra in linearly polarized light showed that the situation is not so clear-cut. Fig. S3 shows the optical density spectra at T=300 K and T=5 K in linearly polarized light. Together with the dependences $D(\mathscr{E})$ (panels a, d) shown in Fig. 3 of the article, the same spectra are shown in Tauc coordinates: on the left – for **E** ∥ **a**, on the right – for **E** ∥ **b**. It can be seen that in the spectra measured at **E** ∥ **a** and plotted in coordinates $(D\mathscr{E})^{1/2}$ vs. $\mathscr{E}$ (Fig. S3c), it is not possible to find an extended linear region that makes it possible to determine the band gap. At the same time, on each of the experimental curves plotted in coordinates $(D\times\mathscr{E})^2$ vs. $\mathscr{E}$, at least two linear sections are visible in the considered spectral range (Fig. S3b). Extrapolation of regions located lower in energy to the x-axis gives a bandgap value of ~1.1 eV at room temperature and 1.18 eV at 5 K. For the direction of light polarization along the **b** axis of the crystal, linear regions are observed both in Fig. S3e, and in Fig. S3f. The band gap estimated from extrapolation of these regions to the x-axis is 0.98 eV at 300 K and 1.02 eV at 5 K in the case of direct transitions (Fig. S3e). If the transitions are indirect, the corresponding values are 0.91 and 0.96 eV (Fig. S3f).

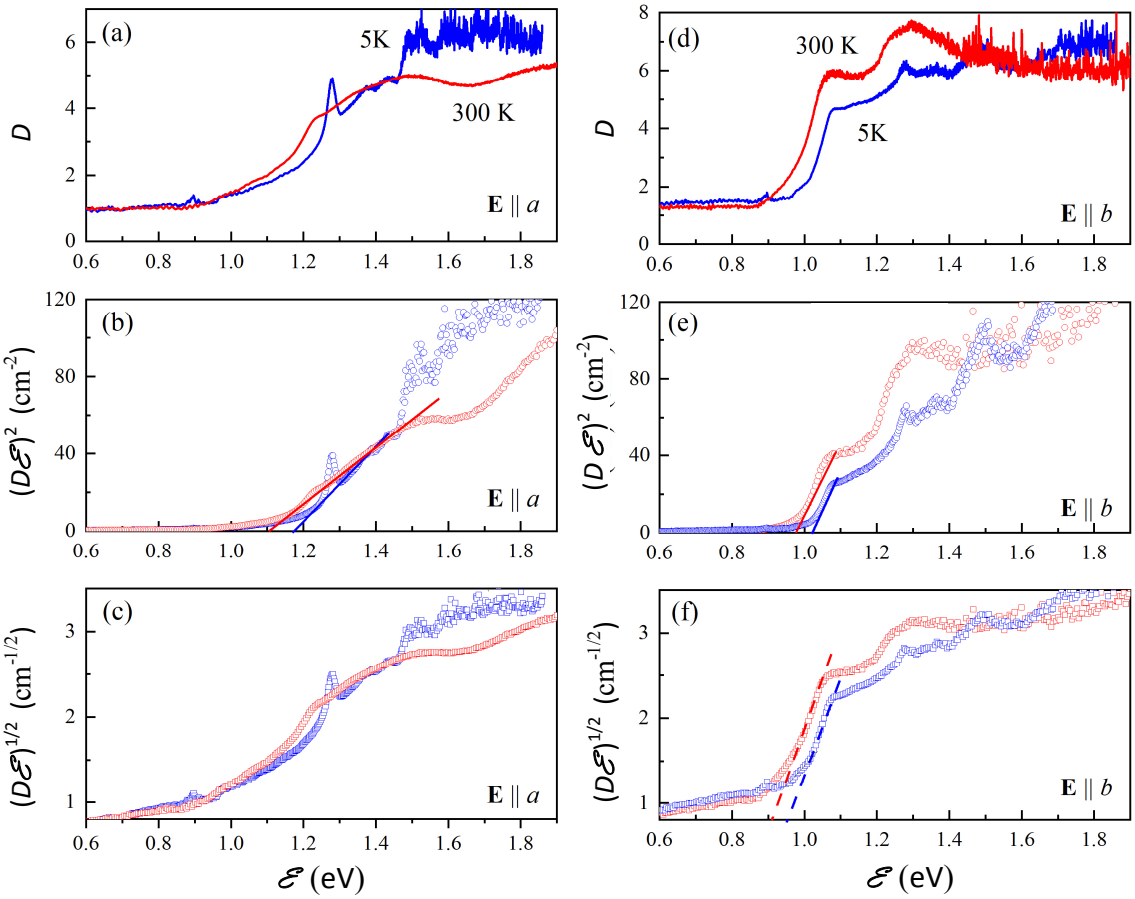

Fig. S3. Optical density spectra (a, d) (see Fig. 3 in the article), and spectra plotted in coordinates $(D\mathscr{E})^2$ vs. $\mathscr{E}$ (b, e) and $(D\times\mathscr{E})^{1/2}$ vs. $\mathscr{E}$ (c, f) of the TiS_3 single crystal # 1, measured at T=300 K (red curves) and 5 K (blue curves) in linearly polarized light directed along the **a**-axis (a, b, c) and **b**-axis (d, e, f) of the crystal .

Thus, we see that the Tauc-plot approach does not allow us to establish the nature of interband transitions. From previous works that examined the nature of transitions [4-19], it is also impossible to draw an unambiguous conclusion.

1. S. Jandl, J. Deslandes and M. Banville, Infrared Phys. **22**, 327 (1982).
2. S.P. Gwet, Y. Mathey, and C. Sourisseau, Phys. stat. sol. (b) **123**, 503 (1984).

3. J.I. Pankove. Optical processes in semiconductors, 2nd edn (N.Y., Dover Publ., 1975).
4. H. Yi, T. Komesu, S. Gilbert, G. Hao, A.J. Yost, A. Lipatov, A. Sinitskii, J. Avila, C. Chen, M.C. Asensio, and P. A. Dowben, Appl. Phys. Lett. **112**, 052102 (2018).
5. A.J. Molina-Mendoza, M. Barawi , R. Biele , E. Flores , J.R. Ares, C. Sánchez, G. Rubio-Bollinger, N. Agraït , R.D'Agosta, I.J. Ferrer, and A. Castellanos-Gomez, Adv. Electron. Mater. **1**, 1500126 (2015).
6. J. Dai, X.C. Zeng, Angew. Chem. Int. Ed. **54**, 7572 (2015).
7. S. Hou, Z. Guo, J. Yang, Y.-Y. Liu, W. Shen, C. Hu, Sh. Liu, H. Gu, and Z. Wei, Small **17**, 2100457 (2021).
8. J.O. Island, A.J. Molina-Mendoza, M. Barawi, R. Biele, E. Flores, J.M. Clamagirand, J.R. Ares, C. Sánchez, H.S.J. van der Zant, R. D'Agosta, I.J. Ferrer and A. Castellanos-Gomez,.2D Mater. **4**, 022003 (2017).
9. J. Kang, L.-W. Wang, Phys. Chem. Chem. Phys., **18**, 14805 (2016).
10. Y. Jin, X. Li and J.Yang, Phys. Chem. Chem. Phys. **17**, 18665 (2015).
11. I.J. Ferrer, J.R. Ares, J.M. Clamagirand, M. Barawi, C. Sánchez, Thin Solid Films **535**, 398 (2013).
12. M. Abdulsalam, D.P. Joubert, Phys. Status Solidi B **253**, 868 (2016).
13. O. Gorochov, A Katty, N. Le Nagard, C. Levy-Clement, D.M. Schleich, Materials Research Bulletin, **18**, 111 (1983).
14. I.J. Ferrer, M.D. Macia, V. Carcelen, J.R. Ares, and C. Sanchez, Energy Procedia **22**, 48 (2012)
15. Z. Lian, Z. Jiang, T. Wang, M. Blei, Y. Qin, M. Washington, T.-M. Lu, S. Tongay, Sh. Zhang, and Su-Fei Shi. Appl. Phys. Lett. **117**, 073101 (2020).
16. J. Wu, D. Wang, H. Liu, W.-M. Laua, Li-Min Liu, RSC Adv. **5**, 21455 (2015).
17. R. Biele, E. Flores, J.R. Ares, C. Sanchez, I. J. Ferrer, G. Rubio-Bollinger, A. Castellanos-Gomez, and R. D'Agosta, Nano Research **11**, 225 (2018).
18. F. Iyikanat, H. Sahin, R.T. Senger, F. Peeters, J. Phys. Chem. C **119**, 19, 10709 (2015).
19. E. Flores, J.R. Ares, I.J. Ferrer, and C. Sánchez, Phys. Status Solidi RRL **10**, 802 (2016).